Am J Physiol Renal Physiol 304: F522–F532, 2013.
First published December 26, 2012; doi:10.1152/ajprenal.00394.2012.

Altered V-ATPase expression in renal intercalated cells isolated from B1 subunit-deficient mice by fluorescence-activated cell sorting

Luca Vedovelli,[1,2] John T. Rothermel,[1] Karin E. Finberg,[3] Carsten A. Wagner,[4] Anie Azroyan,[1] Eric Hill,[1] Sylvie Breton,[1] Dennis Brown,[1] and Teodor G. Păunescu[1]

[1]*Center for Systems Biology, Program in Membrane Biology and Division of Nephrology, Massachusetts General Hospital and Harvard Medical School, Boston, Massachusetts;* [2]*Department of Pharmacology and Anesthesiology, University of Padova, Padova, Italy;* [3]*Department of Pathology, Duke University School of Medicine, Durham, North Carolina; and* [4]*Institute of Physiology and Zürich Center for Integrative Human Physiology, University of Zürich, Zürich, Switzerland*

Submitted 16 July 2012; accepted in final form 20 December 2012

Vedovelli L, Rothermel JT, Finberg KE, Wagner CA, Azroyan A, Hill E, Breton S, Brown D, Păunescu TG. Altered V-ATPase expression in renal intercalated cells isolated from B1 subunit-deficient mice by fluorescence-activated cell sorting. *Am J Physiol Renal Physiol* 304: F522–F532, 2013. First published December 26, 2012; doi:10.1152/ajprenal.00394.2012.—Unlike human patients with mutations in the 56-kDa B1 subunit isoform of the vacuolar proton-pumping ATPase (V-ATPase), B1-deficient mice (Atp6v1b1$^{-/-}$) do not develop metabolic acidosis under baseline conditions. This is due to the insertion of V-ATPases containing the alternative B2 subunit isoform into the apical membrane of renal medullary collecting duct intercalated cells (ICs). We previously reported that quantitative Western blots (WBs) from whole kidneys showed similar B2 protein levels in Atp6v1b1$^{-/-}$ and wild-type mice (Păunescu TG, Russo LM, Da Silva N, Kovacikova J, Mohebbi N, Van Hoek AN, McKee M, Wagner CA, Breton S, Brown D. *Am J Physiol Renal Physiol* 293: F1915–F1926, 2007). However, WBs from renal medulla (including outer and inner medulla) membrane and cytosol fractions reveal a decrease in the levels of the ubiquitous V-ATPase E1 subunit. To compare V-ATPase expression specifically in ICs from wild-type and Atp6v1b1$^{-/-}$ mice, we crossed mice in which EGFP expression is driven by the B1 subunit promoter (EGFP-B1$^{+/+}$ mice) with Atp6v1b1$^{-/-}$ mice to generate novel EGFP-B1$^{-/-}$ mice. We isolated pure IC populations by fluorescence-assisted cell sorting from EGFP-B1$^{+/+}$ and EGFP-B1$^{-/-}$ mice to compare their V-ATPase subunit protein levels. We report that V-ATPase A, E1, and H subunits are all significantly downregulated in EGFP-B1$^{-/-}$ mice, while the B2 protein level is considerably increased in these animals. We conclude that under baseline conditions B2 upregulation compensates for the lack of B1 and is sufficient to maintain basal acid-base homeostasis, even when other V-ATPase subunits are downregulated.

vacuolar H^+-ATPase; proton pump; urinary acidification; pH homeostasis; Atp6v1b1$^{-/-}$ mice; collecting duct

THE PROCESSES OF INTRACELLULAR organelle acidification and extracellular pH regulation via proton transport are fulfilled by a ubiquitous multisubunit enzyme, the vacuolar (V)-ATPase. The expression of specific subunit patterns determines the localization and functions of the enzyme in different organelles, cell types, and even different subcellular or membrane domains within the same cell (14). Renal medullary collecting duct (CD) intercalated cells (ICs) are the major cell type involved in physiological urine acidification and recovery from acidosis and alkalosis. ICs maintain systemic pH homeostasis by reorganizing the polarized distribution of V-ATPase in their plasma membrane domains. During acidosis, V-ATPase accumulates in the apical membrane of A-type ICs while during alkalosis the enzyme is endocytosed into subapical vesicles to reduce urinary acidification. In B-type ICs, the V-ATPase is inserted into the basolateral membrane to reverse the direction of proton secretion to correct alkalosis (2–4, 40).

The B1 subunit of the V_1 cytosolic domain of the V-ATPase (ATP6V1B1) is expressed in kidney ICs, clear cells of the epididymis, nonciliated airway epithelial cells, and in several cell types of the inner ear and olfactory epithelium (8, 26, 33, 35, 37, 42). In humans, mutations of the gene encoding for the B1 subunit (Atp6v1b1) cause distal renal tubular acidosis (dRTA) and deafness (25, 43). dRTA due to ATP6V1B1 mutations is an autosomal recessive disease characterized by an impaired secretion of H^+ by the distal nephron, which leads to metabolic acidosis, hypokalemia, nephrocalcinosis, bone disease, and growth retardation (5, 43). B1-deficient (Atp6v1b1$^{-/-}$) mice were previously generated (18) to investigate the physiological mechanism of dRTA with surprising results. These mice did not develop spontaneous dRTA and had morphologically and functionally normal kidneys under physiological conditions due to a compensatory effect of the B2 isoform, which assembled into plasma membrane V-ATPases (38). We reported a twofold increase in the intensity of the apical B2-associated immunostaining in Atp6v1b1$^{-/-}$ mice and no significant upregulation of B2 mRNA or protein levels in whole kidneys of B1-deficient compared with wild-type mice. However, a more in-depth analysis revealed an impaired capacity of ICs to overcome an acid load (18, 38) or to be stimulated by angiotensin II (39), suggesting that the B2 substitution does not fully compensate for the lack of the B1 isoform.

In the present study, we investigated whether V-ATPase subunit protein levels change in B1-deficient mice in the CD. Immunoblotting of membrane and cytosol fractions from the renal medulla (outer and inner medulla) reveals a downregulation in V-ATPase expression. We then quantified V-ATPase subunit expression specifically in ICs to determine whether the B2 subunit (ATP6V1B2) is in fact upregulated, but the response was masked in our previous study at the whole organ level by contributions from other tubules (such as B2-rich proximal tubules and thick ascending limbs) (33). For this purpose, we generated a new animal model by crossing mice that specifically express enhanced green fluorescent protein (EGFP) in ICs (26) with B1-deficient mice (17, 18). Pure IC populations were isolated from B1-expressing and B1-deficient

Address for reprint requests and other correspondence: T. G. Păunescu, Program in Membrane Biology/Div. of Nephrology, Massachusetts General Hospital, Simches Research Center, 185 Cambridge St., CPZN8150, Boston, MA 02114 (e-mail: Paunescu.Teodor@mgh.harvard.edu).

mice by fluorescence-assisted cell sorting (FACS). This allowed us to determine that ubiquitous A (ATP6V1A), E1 (ATP6V1E1), and H (ATP6V1H) V-ATPase subunits are downregulated in renal ICs from B1-deficient mice whereas the B2 subunit isoform is upregulated.

MATERIALS AND METHODS

Antibodies. To characterize V-ATPase localization in renal CD ICs by immunofluorescence, we used affinity-purified V-ATPase antibodies raised in chicken against the 56-kDa B2 subunit isoform (16) and in rabbit against the 70-kDa A subunit (24). To compare the animal models used in this study, we used an affinity-purified rabbit polyclonal (IgG) antibody raised against rat anion exchanger 1 (AE1; Alpha Diagnostic International, San Antonio, TX) as a marker for A-type ICs of the CD and an affinity-purified goat polyclonal (IgG) antibody raised against human pendrin (Santa Cruz Biotechnology, Santa Cruz, CA) as a marker for B-type ICs. A mouse monoclonal calbindin (IgG1) antibody (Sigma-Aldrich, St. Louis, MO) was used as a distal tubule and connecting segment marker to help identify cortical CDs.

To investigate V-ATPase expression by immunoblotting, we used, besides the A and B2 subunit antibodies described above, previously characterized antibodies raised in rabbit against the 56-kDa B1 subunit isoform (35) and in chicken against the 31-kDa E1 subunit isoform (9, 23). A new polyclonal antibody was raised against a peptide corresponding to the 15 COOH-terminal amino acids of the human V-ATPase 50-kDa H subunit sequence coupled to the keyhole limpet hemocyanin via a cysteine residue. The peptide was synthesized by the Massachusetts General Hospital Peptide/Protein Core Facility, and two rabbits were immunized by Cocalico Biologicals (Reamstown, PA). Immune sera were affinity-purified against the immunizing peptide using a SulfoLink kit (Pierce, Rockford, IL) per the manufacturer's instructions. An affinity-purified goat polyclonal (IgG) antibody raised against human aquaporin-2 (AQP2; Santa Cruz Biotechnology) was used as a marker of CD principal cells. Purified mouse monoclonal (IgG) antibodies raised against chicken or human actin (Sigma-Aldrich and EMD Millipore, Billerica, MA) and human α-actinin (EMD Millipore) were used as loading controls.

The following secondary antibodies were used in this study: affinity-purified indocarbocyanine (Cy3)-conjugated donkey anti-chicken IgY, anti-goat IgG, and anti-rabbit IgG (Jackson ImmunoResearch Laboratories, West Grove, PA), a highly cross-absorbed Alexa Fluor 647 goat anti-mouse IgG (Life Technologies, Grand Island, NY), horseradish peroxidase (HRP)-conjugated donkey anti-chicken IgY and anti-mouse IgG (Jackson ImmunoResearch Laboratories), sheep anti-mouse IgG (Amersham, GE Healthcare, Fairfield, CT), rabbit anti-chicken IgY (Sigma-Aldrich), donkey anti-rabbit IgG (Amersham), and mouse anti-rabbit IgG (Sigma-Aldrich).

Tissue preparation. Adult male mice (30–35 g), wild-type (C57BL6, Jackson Laboratory, Bar Harbor, ME) and B1-deficient ($Atp6v1b1^{-/-}$), were housed under standard conditions and maintained on a standard diet with free access to water. Generation, breeding, and genotyping of the original $Atp6v1b1^{-/-}$ founders have been described elsewhere (18). Generation of the GFP-expressing $Atp6v1b1^{-/-}$ mice will be described in RESULTS. All animal studies were approved by the Massachusetts General Hospital Subcommittee on Research Animal Care, in accordance with the National Institutes of Health, Department of Agriculture, and AAALAC requirements, or by the local Swiss Veterinary Authority (Veterinäramt, Zürich, Switzerland), in accordance with Swiss Animal Welfare Laws. For immunofluorescence experiments, mice were anesthetized using pentobarbital sodium (50 mg/kg body wt ip, Nembutal, Abbott Laboratories, Abbott Park, IL) and perfused for 1–2 min through the left cardiac ventricle with PBS (0.9% NaCl in 10 mM phosphate buffer, pH 7.4), followed by paraformaldehyde-lysine-periodate fixative (PLP; 4% paraformaldehyde, 75 mM lysine-HCl, 10 mM sodium periodate, and 0.15 M sucrose, in 37.5 mM sodium phosphate) for 5 min, as previously described (33). Both kidneys were dissected, sliced, and further fixed by immersion in PLP for 4 h at room temperature and subsequently overnight at 4°C, then rinsed extensively in PBS, and stored at 4°C in PBS containing 0.02% sodium azide until use.

Immunofluorescence. PLP-fixed kidney slices (1–2 mm) prepared as described above were cryoprotected in PBS containing 0.9 M sucrose overnight at 4°C and then embedded in Tissue-Tek OCT compound 4583 (Sakura Finetek USA, Torrance, CA), mounted on a specimen disk, and frozen at −20°C (34, 38). Sections (4 μm) were cut on a Leica CM3050 S cryostat (Leica Microsystems, Bannockburn, IL), collected onto Superfrost Plus precleaned charged microscope slides (Thermo Fisher Scientific, Rockford, IL), air-dried, and stored at 4°C until use. Sections were rehydrated for 3 × 5 min in PBS and treated with 1% (wt/vol) SDS for 4 min for retrieval of antigenic sites (13). After being washed for 3 × 5 min in PBS and incubated for 10 min in 1% (wt/vol) BSA in PBS with 0.02% sodium azide to reduce nonspecific staining, the sections were incubated for 90 min with the primary antibody diluted in Dako antibody diluent (Dako, Carpinteria, CA) at room temperature, as described previously (33–35). After 3 × 5-min PBS washes, the secondary antibody was applied for 1 h at room temperature and the slides were then rinsed again in PBS for 3 × 5 min. Slides were mounted in Vectashield medium with 4,6-diamidino-2-phenylindole (DAPI) as a nuclear stain (Vector Laboratories, Burlingame, CA) for microscopy and image acquisition. Digital images were acquired as described previously (33, 35) by using a Nikon 80i epifluorescence microscope (Nikon Instruments, Melville, NY) equipped with an Orca 100 CCD camera (Hamamatsu, Bridgewater, NJ). Epifluorescence images were analyzed using IPLab version 3.9.5 r2 image-processing software (BD Biosciences, San Jose, CA) and then imported into and printed from Adobe Photoshop version 9.0.2 image-editing software (Adobe Systems, San Jose, CA).

Apical immunofluorescence staining for the V-ATPase B2 subunit was quantified as previously described in detail (38). Sections from three B1-expressing and three B1-deficient mice were immunostained, and digital images were acquired under identical conditions, including same exposure time (150 ms). Immunostained areas were selected using the segmentation function in IPLab version 3.9.5 r2, and their mean pixel intensity (MPI) was measured. Statistical analysis of MPI data was performed in Excel version 12.3.4 (Microsoft, Redmond, WA) to express the summary data as means ± SD and in Prism 4 for MacIntosh version 4.0c (GraphPad Software, La Jolla, CA) to assess statistical significance using the unpaired Student's *t*-test. The same statistical analysis was performed for all other measurements reported in this study.

Fluorescence-activated cell sorting of B1-expressing cells from the kidney. Isolated cells were prepared using a variation of a previously
described method (36). Mice were anesthetized using isoflurane (Baxter, Deerfield, IL) and euthanized. Kidneys were dissected and minced immediately with scissors in prewarmed RPMI 1640 medium (GIBCO Invitrogen, Carlsbad, CA) containing 1 mg/ml collagenase type I (GIBCO Invitrogen), 1 mg/ml collagenase type II, and 1 mg/ml hyaluronidase (Sigma-Aldrich). Tissue dissociation was performed for 45 min in a 2D shaker (1,400 rpm for 10 s every minute) at 37°C. Cell preparations were then passed through a cell strainer with 40-μm nylon mesh to remove undigested material, and cells were washed once with RPMI 1640 medium and once with calcium-free phosphate-buffered saline (DPBS). Immediately before sorting, cells were suspended in a sterile filtered (0.22 μm) medium containing 5 mM EDTA, 25 mM HEPES, 1% DNase I 50 μg/ml FBS, and 0.1% DEPC, and filtered (40-μm nylon mesh) into a capped tube to eliminate cells clumps. Populations of EGFP-positive (EGFP+) cells from kidney preparations were isolated immediately by FACS based on their green fluorescence intensity. Sorting was performed using a modified

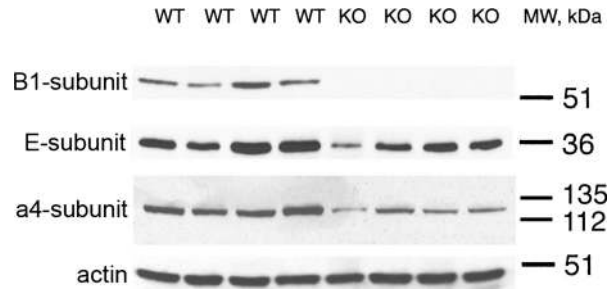

Fig. 1. Immunoblotting results for the membrane fraction of the renal medulla (including outer and inner medulla) from 4 Atp6v1b1$^{+/+}$ (WT) and 4 Atp6v1b1$^{-/-}$ mice (KO) screened with antibodies against the V-ATPase B1 (ATP6V1B1), E1 (ATP6V1E1), and a4 (ATP6V0A4) subunit isoforms. Loading control was performed with an anti-actin antibody. Pixel quantification reveals that E1 and a4 band intensities normalized to actin are decreased by ~50% in B1-deficient compared with WT mice. The B1 subunit is, as expected, not detectable in the Atp6v1b1$^{-/-}$ mice.

FACSVantage cell sorter (BD Biosciences) with DIVA option. EGFP+ and EGFP-negative cell samples were collected in Dulbecco's PBS and used without delay for protein isolation. Cells with intermediate to low fluorescence intensity were discarded to avoid potential contamination of cells that were negative for EGFP, but had a high autofluorescence, in the EGFP+ cell preparation. A fraction of each cell sample was reanalyzed by flow cytometry to estimate the purity (>95%).

Subcellular fractionation. Cells were fractionated using the protocol suggested by Abcam (www.abcam.com/ps/pdf/protocols/subcellular_fractionation.pdf; Abcam USA, Cambridge, MA) with one modification: Complete Mini (F. Hoffmann-La Roche, Basel, Switzerland) was used as protease inhibition cocktail instead of PI Cocktail (III) (Abcam). Briefly, the subfractionation buffer consisted of: 150 mM sucrose, 20 mM HEPES pH 7.4, 10 mM KCl, 1.5 mM $MgCl_2$, 1 mM EDTA, 1 mM EGTA, 1 mM DTT, and 1 tablet of Complete Mini/10 ml of solution. Cells were lysed in the subfractionation buffer, centrifuged at 720 and 10,000 *g* to eliminate nuclei and mitochondria, and then twice at 100,000 *g* for 1 h to separate cytosolic and membrane fractions.

Western blot analysis. For immunoblot analysis of the renal medulla, mice were anesthetized as described above and euthanized. Transverse sections of the kidney were cut with a razor blade, and the cortex was separated from the medulla under a microscope, using the arcuate arteries as a landmark running between the cortex and outer medulla. Microdissected medullas were homogenized in ice-cold K-HEPES buffer (200 mM mannitol, 80 mM K-HEPES, 41 mM KOH, pH 7.5) with 100 μM each pepstatin, leupeptin, K-EDTA, and phenylmethylsulfonyl fluoride added as protease inhibitors. After centrifugation at 1,000 *g* for 10 min at 4°C, the recovered supernatant was further centrifuged at 100,000 *g* for 1 h at 4°C; the final supernatant (cytosolic fraction) was saved, and the membrane pellets were resuspended in K-HEPES buffer containing protease inhibitors. After determination of the total protein concentration using a Bio-Rad Protein Assay (Bio-Rad Laboratories, Hercules, CA), membrane proteins were solubilized in Laemmli reducing sample buffer (Bio-Rad), fractionated by SDS-PAGE, and transferred electrophoretically to Immobilon-P polyvinylidene difluoride (PVDF) membranes (EMD Millipore). Fifty micrograms of cortical membrane protein, 25 μg of medullary membrane protein, or 25 μg medullary cytosolic protein were loaded per lane. After blocking with Tris-buffered saline (TBS) containing 0.1% Tween 20 and 5% nonfat dry milk, blots were incubated with primary antibody for either 2 h at room temperature or overnight at 4°C. After washing and subsequent blocking, blots were incubated with horseradish peroxidase (HRP)-conjugated secondary antibody for 1 h at room temperature.

For GFP-expressing cell analysis, 500,000 cells were isolated by FACS from each mouse as described above. Cells were then lysed in RIPA buffer (30 min at 4°C, Boston BioProducts, Ashland, MA) supplemented with protease inhibitors (Complete Mini, Roche). Total wild-type mouse kidney and epididymis protein extracts were prepared as previously described (38). Protein concentration was determined with the bicinchoninic acid protein assay (Pierce Biotechnology) using albumin as a standard; 2.2 μg of protein were diluted in Laemmli buffer as described above, heated at 65°C for 15 min, and loaded onto Tris-glycine polyacrylamide 4–20% gradient gels (Bio-Rad). After SDS-PAGE separation, proteins were transferred onto an Immun-Blot PVDF membrane (Bio-Rad), and the membrane was blocked in TBS containing 5% nonfat dry milk at room temperature for 2 h, and incubated overnight at 4°C with the primary antibody diluted in TBS containing 2.5% dry milk. The membrane was subsequently washed and incubated with a secondary antibody conjugated to HRP as described above and previously reported (34, 38).

Following additional washes, antibody binding was detected with Western Lightning chemiluminescence reagent (PerkinElmer Life Sciences, Boston, MA) using Kodak film. For quantitative analysis of protein bands from immunoblotting experiments, digital images of the membranes were acquired using an Epson Perfection 4990 (Epson America, Long Beach, CA) imaging system, and band optical densities were quantified from scanned films using ImageJ software (version 1.42q, National Institutes of Health, Bethesda, MD). To account for possible sample loading variations, actin or α-actinin bands were analyzed in a similar fashion, and quantification of all V-ATPase subunit protein bands included normalization to the respective actin or α-actinin controls. To ensure that the proteins used were appropriate controls (i.e., not modulated due to the B1 deficiency), we also checked for equal loading by staining initial gels with Coomassie blue (Thermo Fisher Scientific).

RESULTS

Western blot analysis of renal medullas from wild-type and B1-deficient mice. To assess the expression patterns of V-ATPase subunits in the renal medulla of B1-deficient (Atp6v1b1$^{-/-}$) compared with wild-type mice, we dissected the medullary region (including outer and inner medulla) from four mice from the two groups and performed Western blot analysis using both membrane and cytosolic fractions. As expected, Atp6v1b1$^{-/-}$ mice were confirmed as such by the absence of B1 protein (ATP6V1B1, Fig. 1). Immunoblotting of the membrane fraction from renal medullas revealed a decrease in the levels of the V-ATPase E1 (ATP6V1E1) and a4 (ATP6V0A4) subunit levels in Atp6v1b1$^{-/-}$ mice compared with their wild-type counterparts (Fig. 1). Similarly, the 31-kDa E subunit (E1 subunit isoform) is also expressed at lower levels in the cytosolic fraction of renal medullas from Atp6v1b1$^{-/-}$

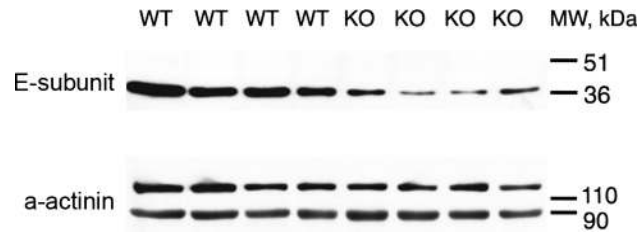

Fig. 2. Detection of the V-ATPase E1 subunit (ATP6V1E1) in the cytosolic fraction of the renal medulla (including outer and inner medulla) from 4 Atp6v1b1$^{+/+}$ (WT) and 4 Atp6v1b1$^{-/-}$ mice (KO). Loading control was performed with an anti-α-actinin antibody. The intensity of the E1 band normalized to that of the α-actinin band is reduced by ~60% in B1-deficient compared with WT mice.

mice (Fig. 2), indicating an overall downregulation of this ubiquitous subunit. The pixel quantification performed using ImageJ revealed that the E1 band intensity (normalized to the respective actin control) is decreased on average by 53% in the membrane fraction from Atp6v1b1$^{-/-}$ mice, from 0.754 ± 0.140 (mean ± SD, n = 4 wild-type mice) to 0.346 ± 0.036 (mean ± SD, n = 4 Atp6v1b1$^{-/-}$ mice) (Fig. 1). This decrease is statistically significant, as revealed by Student's t-test (P = 0.0013). A similar quantification indicated that in the cytosolic fraction the normalized E1 band intensity is also significantly decreased in these animals, by 56%, from 0.627 ± 0.114 (n = 4 wild-type mice) to 0.278 ± 0.081 (n = 4 Atp6v1b1$^{-/-}$ mice) (P = 0.0025) (Fig. 2). These results prompted us to investigate V-ATPase subunit levels specifically in CD ICs in the presence and absence of the B1 isoform.

Hybrid EGFP-expressing B1-deficient mice. To address this issue, we generated a new animal model, by crossing mice in which EGFP expression is driven by the Atp6v1b1 promoter (EGFP-B1$^{+/+}$ mice) (26), with B1-deficient mice (18) to generate Atp6v1b1$^{-/-}$ mice that express EGFP in ICs of the CD (EGFP-B1$^{-/-}$ mice). As expected, the first round of breeding produced EGFP-expressing offspring that were heterozygous for Atp6v1b1. These mice were subsequently interbred, producing Atp6v1b1$^{+/+}$, $^{+/-}$, and $^{-/-}$ pups, most of which also expressed EGFP in ICs. The EGFP-expressing B1-deficient animals (EGFP-B1$^{-/-}$) were used as founders for a colony that was established and is currently maintained at the Massachusetts General Hospital as described in MATERIALS AND METHODS. As previously reported for the B1-deficient mice (18), EGFP-B1$^{-/-}$ mice are as viable as wild-type mice, and they grow, behave, and breed normally, being fully fertile.

To characterize this mouse model, we used immunostaining with antibodies against the B2 (ATP6V1B2) and A subunits of the V-ATPase (ATP6V1A) to confirm the EGFP expression in virtually all CD ICs from all kidney regions, including the inner medulla (Fig. 3), the outer medulla (Fig. 4), and cortex (Fig. 5). EGFP expression in the CD from EGFP-B1$^{-/-}$ mice is detected exclusively in the ICs, as previously reported for EGFP-B1$^{+/+}$ mice, in which B1 expression overlaps with GFP expression (26). On the other hand, V-ATPase expression levels are visibly higher in ICs than in neighboring principal cells (PCs), as described previously (33). Moreover, we found the subcellular V-ATPase localization in A-ICs from EGFP-B1$^{+/+}$ mice to be the same as in wild-type mice (33, 38), the enzyme being expressed at higher levels in the cytosolic region located between the apical plasma membrane and the cell nucleus (B2 subunit: Figs. 3*B* and 5*B*, A subunit: Fig. 4*B*). In contrast, V-ATPase immunostaining was significantly more polarized in A-ICs from EGFP-B1$^{-/-}$ mice (B2 subunit: Figs. 3*E* and 5*E*, A subunit: Fig. 4*E*), as previously reported for the original B1-deficient animals (18, 38). The A and B2 subunits exhibit the same subcellular localization pattern in these animals, both being concentrated in a narrower and brighter band of apical membrane staining. As previously described for non-EGFP-expressing animals (38), we quantified the mean pixel intensity (MPI) of the apical B2 immunostaining in EGFP-B1$^{+/+}$ and EGFP-B1$^{-/-}$ mice (see also MATERIALS AND METHODS). Inner medullary collecting duct A-ICs were identified based on their EGFP expression, and apical MPI was determined for an average of 59 cells/EGFP-B1$^{+/+}$ mouse and 62 cells/EGFP-B1$^{-/-}$ mouse. The MPI increased from 268 ± 29 (mean ± SD, n = 3) in EGFP-B1$^{+/+}$ to 558 ± 129 (mean ± SD, n = 3) in EGFP-B1$^{-/-}$ mice (P = 0.0095), indicating an increase in the B2 levels in the apical membrane domain of ICs in B1-deficient mice, qualitatively and quantitatively similar to the one reported for non-EGFP-expressing animals (38).

To compare the cellular composition of the CD in EGFP-B1$^{+/+}$ and EGFP-B1$^{-/-}$ mice, we immunostained kidney sections from both animal groups with the A-IC marker AE1 and the B-IC marker pendrin. EGFP expression was used as a general IC marker (26), and DAPI was used as a nuclear marker, so that we could calculate the number of PCs as the difference between the total number of cells and EGFP-expressing ICs. The ratio of PCs, A-ICs, and B-ICs was determined by counting cells in cortical CDs (which we distinguished from proximal tubules based on morphology, and from connecting segments and distal convoluted tubules based on calbindin staining) from three EGFP-B1$^{+/+}$ and three EGFP-B1$^{-/-}$ mice, each stained separately with AE1 and pendrin. The cell type percentages were determined for each cortical CD examined, and a mean percentage was calculated for each tissue. These data were subsequently averaged for the EGFP-B1$^{+/+}$ group and respectively for the EGFP-B1$^{-/-}$ group. Overall, >1,100 cells in >50 tubules were counted for each mouse group (between 290 and 471 cells/animal). Our results indicate no significant difference ($P > 0.05$) between the two animal models. The PC percentage was 54.5 ± 1.0% (mean ± SD, n = 3) in EGFP-B1$^{+/+}$ mice and 56.9 ± 2.8% in EGFP-B1$^{-/-}$ mice. Among ICs, the A-IC percentage was 61.4 ± 4.0% (mean ± SD, n = 3) in EGFP-B1$^{+/+}$ mice and 60.7 ± 2.2% in EGFP-B1$^{-/-}$ mice. This statistical analysis was replicated per tissue section (treating AE1- and pendrin-incubated slides separately) and per CCD, both yielding similar numerical results for the PC:A-IC:B-IC ratio and no statistically significant differences between the two animal groups. This finding indicates that CCD architecture is similar in EGFP-B1$^{+/+}$ and EGFP-B1$^{-/-}$ mice, thus confirming our previous report that the CDs maintain a normal cellular composition in B1-deficient mice (18).

Western blot analysis of FACS-isolated ICs. Characteristics and purity of the FACS-isolated kidney cells were described elsewhere (15). In the present study, we found ICs, characterized by EGFP expression (EGFP+ cells), to represent 2–6% of the live cell population isolated from mouse kidneys as described in MATERIALS AND METHODS (Fig. 6). This is similar to the percentage of EGFP+ clear cells isolated in a similar manner from mouse epididymis in a previous report (15). We verified the purity of our preparation by immunoblotting isolated cell lysates with an antibody against AQP2 (Fig. 7). We found no detectable AQP2 expression in our EGFP+ cell samples from EGFP-B1$^{+/+}$ or EGFP-B1$^{-/-}$ mice (Fig. 7, *A* and *C*), consistent with no significant PC contamination. As expected, isolated ICs from EGFP-B1$^{+/+}$ mice express B1 protein, while ICs from EGFP-B1$^{-/-}$ mice do not (Fig. 7*B*).

Characterization of the novel antibody against the H subunit of the V-ATPase. A V-ATPase antibody was raised in rabbits against the H subunit (ATP6V1H) as described in MATERIALS AND METHODS and used in this study to investigate the expression levels for this subunit in IC preparations from EGFP-B1$^{+/+}$ or EGFP-B1$^{-/-}$ mice. We characterized this antibody in immunofluorescence and immunoblotting experiments, as

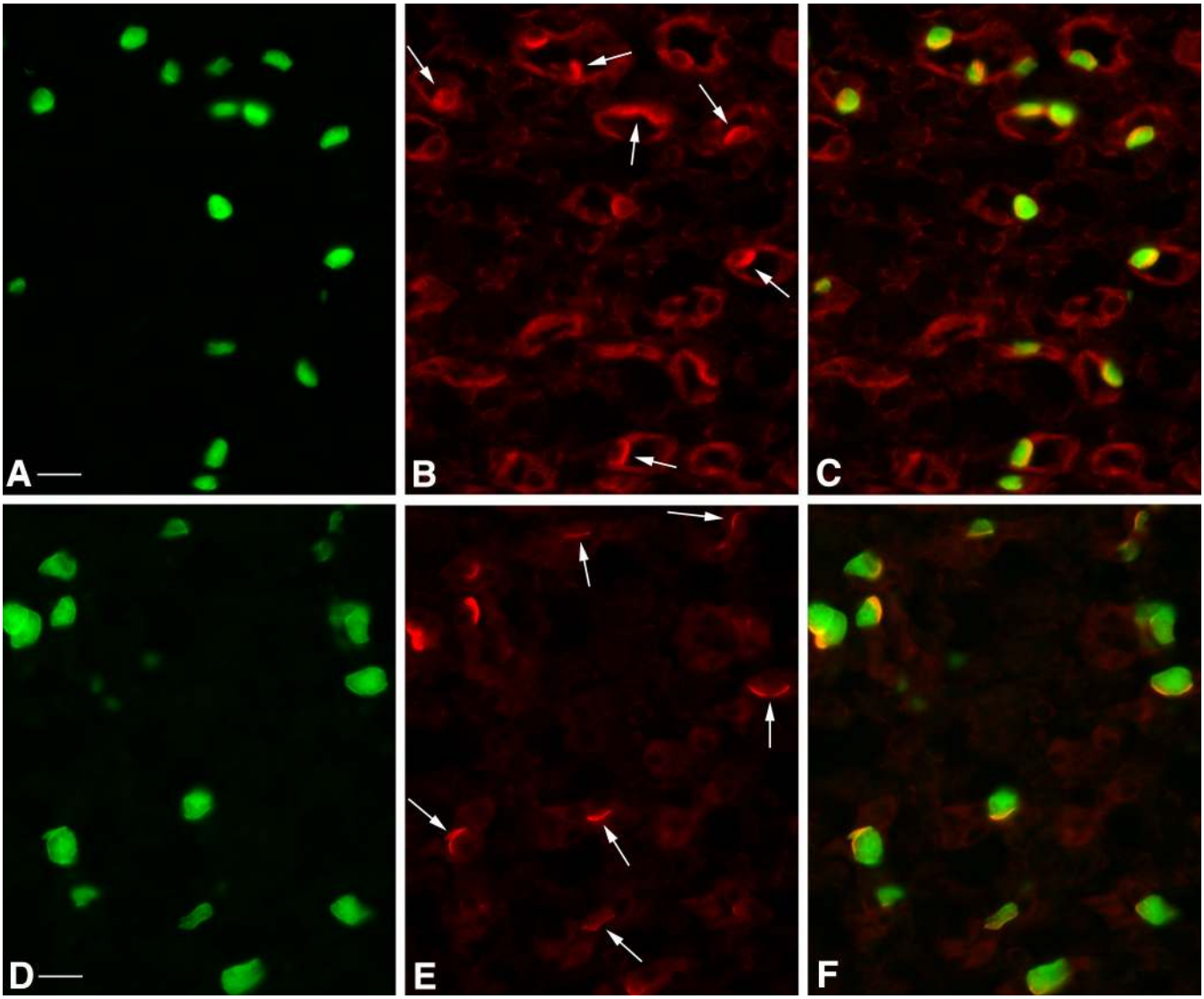

Fig. 3. Generation of B1 null mice expressing enhanced green fluorescent protein (EGFP) in intercalated cells. Shown is immunocytochemical localization of the V-ATPase B2 subunit isoform (ATP6V1B2) in inner medullary collecting ducts from EGFP-B1$^{+/+}$ (*A–C*) and EGFP-B1$^{-/-}$ mice (*D–F*). Intercalated cells, identified based on the EGFP expression (green, *A* and *D*), are more intensely stained for B2 (red) than the adjacent principal cells (*B* and *E*) as clearly seen in the merge panels (*C* and *F*). The subcellular localization of B2 in intercalated cells is diffuse (subapical and cytosolic) in EGFP-B1$^{+/+}$ mice (*B*, arrows) but concentrated in a narrow band of bright apical staining in EGFP-B1$^{-/-}$ mice (*E*, arrows). Scale bars = 30 μm.

well as in peptide competition assays performed as previously described (33). Immunoblotting shows a strong band at 50 kDa, as expected for the H subunit of the V-ATPase. A less intense band was seen below this main band, possibly representing a degradation product. Preincubation with the immunizing peptide abolishes all bands seen under control conditions, attesting to their specificity (Fig. 8).

Further characterization of the antibody was performed by immunofluorescence, which established that it shows the predicted localization of the antigen. The staining was completely inhibited by the immunizing peptide. This assay shows that the same cells that express the V-ATPase B1 subunit isoform also stain for the H subunit, thus localizing it, as expected, to CD ICs (Fig. 9). The H subunit was also detected wherever V-ATPase is known to be expressed, including in the brush-border domain of proximal convoluted tubules (data not shown), where B1 is not expressed, as previously reported (29, 33). Given that the B1 isoform is mostly incorporated into plasma membrane holoenzymes, whereas H is present in all V-ATPases (containing both B1 and the alternative 56-kDa B2 isoform), it is expected that the subcellular localization of B1 should be more apically polarized, while H would be detected not only on the plasma membrane but also in association with organelle membranes. Indeed, our results show that the staining pattern for the antibody raised against the H subunit of the V-ATPase is more diffuse, with a large cytosolic component. The H subunit staining was abolished throughout the kidney upon preincubation of the antibody with its immunizing peptide (Fig. 9).

Quantitative western blot analysis of V-ATPase subunits in FACS-isolated intercalated cells. Western blot analysis for other V-ATPase V_1 subunits indicated a downregulation of the enzyme in ICs from B1-deficient mice. As shown in Fig. 10, band intensities corresponding to the A, E1, and H subunits are

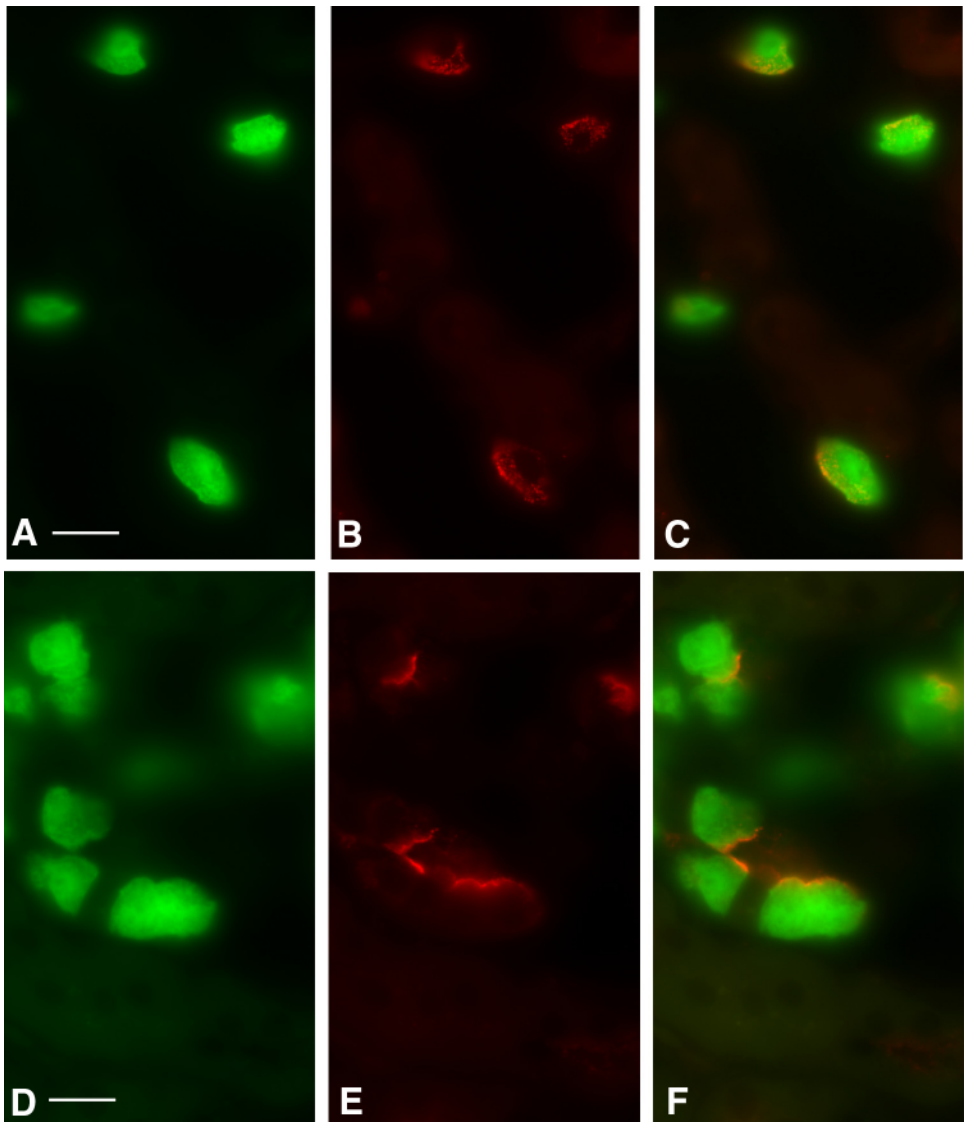

Fig. 4. Immunofluorescence labeling for the V-ATPase A subunit (ATP6V1A) in outer medullary collecting duct intercalated cells from EGFP-B1$^{+/+}$ (*A–C*) and EGFP-B1$^{-/-}$ mice (*D–F*). As seen above for the B2 subunit isoform of the V-ATPase, the subcellular localization of the A subunit (red, *B* and *E*) in EGFP-expressing (green, *A* and *D*) intercalated cells is not only apical, but mostly diffuse (subapical and cytosolic) in EGFP-B1$^{+/+}$ mice (*B*). Conversely, A subunit staining in intercalated cells from EGFP-B1$^{-/-}$ mice is primarily localized to the apical membrane domain. Scale bars = 20 μm.

visibly decreased in EGFP+ cells from EGFP-B1$^{-/-}$ mice compared with EGFP-B1$^{+/+}$ mice. Quantification of band intensities normalized for their respective actin band reveals statistically significant decreases of 59% for A, E1, and H subunits in EGFP-B1$^{-/-}$ mice compared with the average EGFP-B1$^{+/+}$ values (A: from 1.240 ± 0.095 in EGFP-B1$^{+/+}$ to 0.508 ± 0.141 in EGFP-B1$^{-/-}$ mice, means ± SD, $n = 3$, $P = 0.0006$; E1: from 2.535 ± 0.149 to 1.035 ± 0.496, $P = 0.0074$; H: from 0.337 ± 0.016 to 0.147 ± 0.014, $P < 0.0001$). This quantification was repeated in a different group of eight animals ($n = 4$ EGFP-B1$^{+/+}$ and 4 EGFP-B1$^{-/-}$ mice) and the results, shown in Fig. 11, were remarkably similar: V-ATPase subunit band intensities normalized to actin in EGFP-B1$^{-/-}$ mice were reduced by 63% for the A subunit, 62% for E1, and 60% for H. Taken together, these data indicate that immunoblotting band intensities for all three V-ATPase subunits included in this study are downregulated by ~60% in ICs from B1-deficient mice compared with their wild-type counterparts.

Upregulation of the B2 subunit isoform in ICs from B1-deficient mice. Immunoblot analysis for the B2 subunit isoform of the V-ATPase revealed that it is upregulated in ICs from B1-deficient mice (Fig. 12*A*). Quantification of B2 immunoblotting band intensities was performed as described above for other V-ATPase subunits. An initial analysis revealed an increase in the B2 band intensity normalized to actin in B1-deficient mice by 70% (from 0.536 ± 0.243 in EGFP-B1$^{+/+}$ to 0.912 ± 0.059 in EGFP-B1$^{-/-}$ mice, means ± SD, $n = 3$ EGFP-B1$^{-/-}$ and 4 EGFP-B1$^{+/+}$ mice, $P = 0.028$). A repeat experiment confirmed this stimulatory trend, showing a 78% increase in the normalized B2 band intensity in EGFP-B1$^{-/-}$ compared with EGFP-B1$^{+/+}$ mice ($n = 4$) (Fig. 12*B*).

DISCUSSION

The V-ATPase is the ubiquitous enzyme responsible for the translocation of H^+ ions across membranes, whether membranes of intracellular organelles, including endosomes, parts of the Golgi/*trans*-Golgi network, synaptic vesicles, and lysosomes (20, 28, 30) or the plasma membrane in specialized "professional" acid-secreting cells (6, 8, 11, 12, 42). As such, the V-ATPase is the major contributor to the acidification of intracellular organelles, and it is also critical for maintaining

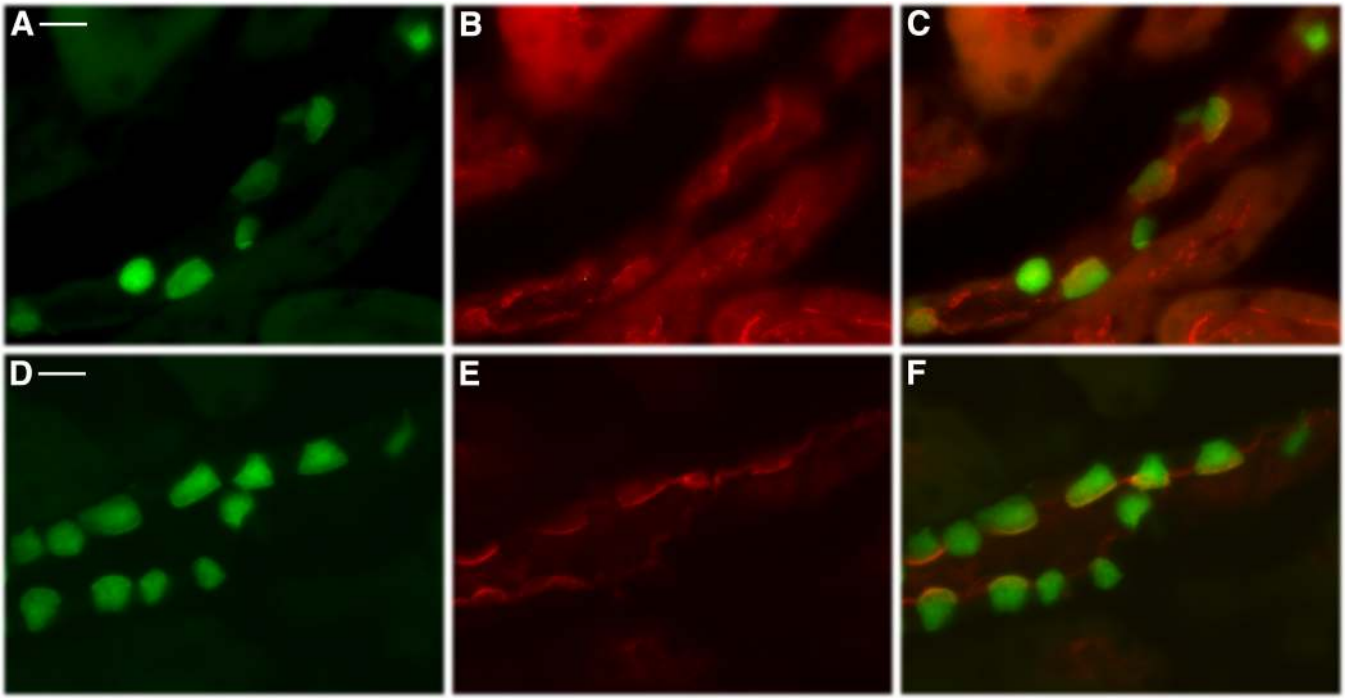

Fig. 5. Subcellular localization of the V-ATPase B2 subunit (ATP6V1B2) in cortical collecting duct intercalated cells identified based on their EGFP expression (green, *A* and *D*). As shown in collecting duct intercalated cells from the inner medulla (Fig. 3), B2 localization (red, *B* and *E*) shifts from the typical pattern seen in WT mice (*A–C*) to a thin bright line of apical staining in EGFP-B1$^{-/-}$ mice (*D–F*). Scale bars = 20 μm.

body acid-base homeostasis, given its presence in the apical and basolateral membrane domain of renal cortical and medullary CD ICs (10, 14, 28, 30, 47). The V-ATPase is a complex, multisubunit holoenzyme (7, 14, 19, 27, 46) in which the assembly of one or more particular subunit isoforms may lead to its different subcellular localization and a cell type-specific response. The mechanisms of biochemical regulation of the holoenzyme in response to specific stimuli are not yet completely elucidated but, as recently shown by us and others, involve mediators such as soluble adenylyl cyclase (sAC), PKA, AMP-activated protein kinase (AMPK), and PKC (1, 10, 14, 21, 22, 32, 34, 36, 48).

Although mutations of the gene encoding for the B1 subunit isoform (Atp6v1b1) were identified as the cause of distal renal tubular acidosis (dRTA) and deafness in humans (25, 43), B1-deficient mice exhibit no phenotype of spontaneous metabolic acidosis and no hearing abnormalities (17, 18, 38). As described before, in these mice the compensatory insertion of the B2 subunit (ATP6V1B2) into IC apical membranes occurs. Despite this, B1-deficient mice cannot handle an acid load appropriately, suggesting a decrease in the maximal V-ATPase ability to excrete protons in the absence of B1 (38). We hypothesized that the milder phenotype seen in B1-deficient mice compared with human patients is due to the mutated human B1 subunit affecting the ability of the alternative B2 subunit isoform to insert into V-ATPase holoenzymes targeted to the membrane domain, and thus compromising V-ATPase activity in humans. In B1-deficient mice, the B1 subunit is not mutated, but is completely absent, and consequently there is no such competition for B2 within the holoenzyme (38). The

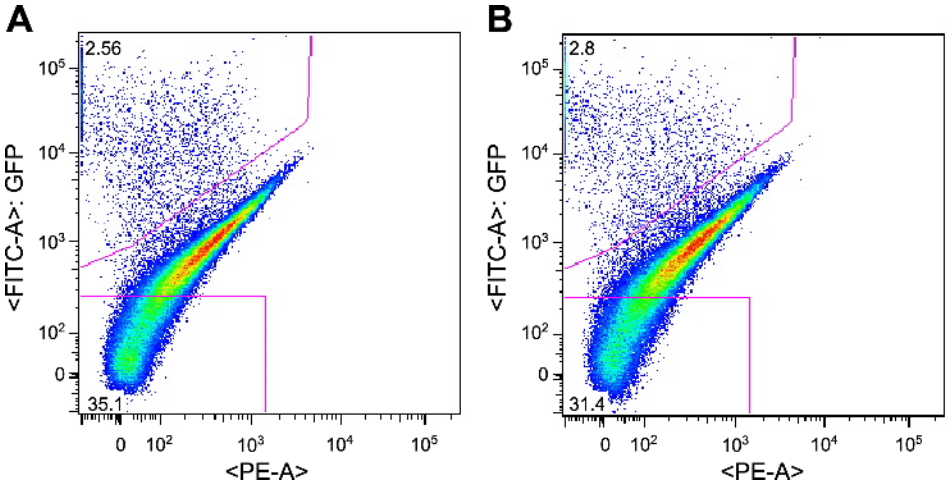

Fig. 6. Fluorescence-assisted cell sorting (FACS) analysis of renal cells from mice expressing EGFP in intercalated cells shown as an EGFP vs. phycoerythrin channel autofluorescence (PE-A) dot plot. Profiles are similar in EGFP-B1$^{+/+}$ (*A*) and EGFP-B1$^{-/-}$ mice (*B*). In these particular cases, the percentages of isolated EGFP-expressing intercalated cells were 2.6% (EGFP-B1$^{+/+}$ mouse) and 2.8% (EGFP-B1$^{-/-}$ mouse). To avoid any possible contamination, only cells exhibiting the highest intensity levels in the EGFP channel were harvested as EGFP-positive cells. Non-EGFP-expressing cells were harvested from the same animals and were defined as cells with low EGFP fluorescence, in this case representing 35.1% (EGFP-B1$^{+/+}$ mouse) and 31.4% (EGFP-B1$^{-/-}$ mouse) of the total cell population.

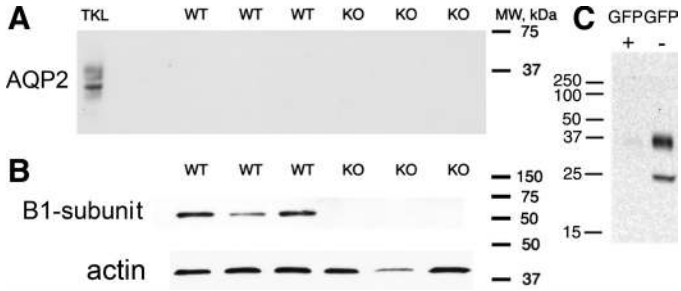

Fig. 7. Intercalated cell populations isolated by FACS based on their EGFP expression contain no detectable levels of the principal cell marker aquaporin-2 (AQP2) in either EGFP-B1$^{+/+}$ (WT) or EGFP-B1$^{-/-}$ mice (KO; *A*), characterized by the lack of expression of the V-ATPase B1 subunit isoform (*B*). AQP2 is detected only in the total kidney lysate (TKL) used as positive control (*A*). To verify that AQP2 was not degraded during the cell isolation or sorting process, we examined an intercalated cell population isolated as EGFP-expressing cells (GFP+) alongside non-EGFP-expressing cells (GFP−) isolated from the same mouse kidney during the same run (*C*). As expected, AQP2 is readily detectable in the principal cell-containing GFP− sample.

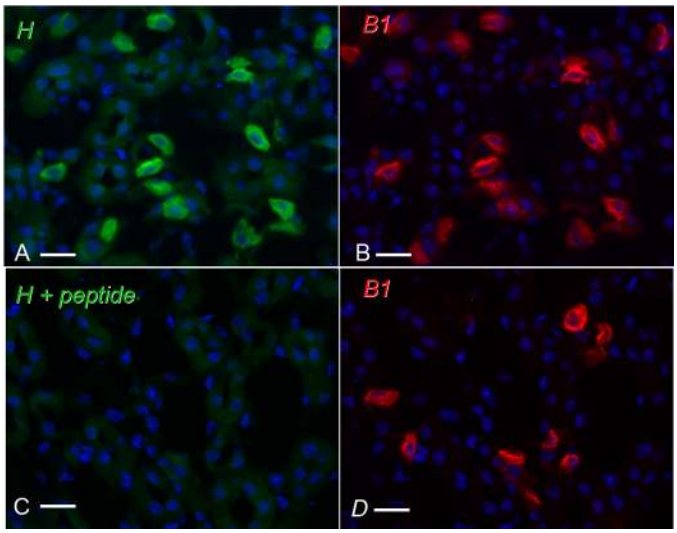

Fig. 9. Characterization of the V-ATPase H subunit (ATP6V1H) antibody by immunofluorescence. The antibody localizes the H subunit (green, *A*) to intercalated cells of the WT mouse inner medullary collecting duct identified by V-ATPase B1 subunit immunostaining (red, *B*). Colocalization of B1 and H subunits in the apical membrane domain and the cytoplasm of intercalated cells is seen by comparing panels *A* and *B*. H subunit staining was abolished when the antibody was preincubated with the immunizing peptide (*C*), while B1 subunit staining was preserved under these circumstances (*D*). 4,6-Diamidino-2-phenylindole (DAPI) marks cell nuclei (blue). Scale bars = 20 μm.

phenotypic difference between humans and mice with B1 mutations might also reflect dietary differences (such as the organic acid composition). It is possible that the B2 isoform cannot fully compensate in humans due to species-specific differences in the regulation of B1/B2 subunit isoform expression or V-ATPase assembly.

The goal of this study was to investigate the regulation of V-ATPase subunits at the protein level in the absence of the B1 isoform. For this purpose, we generated a hybrid animal model by crossing mice expressing EGFP specifically in ICs, driven by the Atp6v1b1 promoter (26), with mice lacking the same B1 subunit isoform (18). This mouse model allows us to use FACS technology to isolate individual EGFP-expressing cells and hence study pure IC preparations. In this way, we could compare and contrast B1-expressing and B1-deficient ICs at the protein or gene level.

Our results reveal that Western blot band intensities for the ubiquitous V-ATPase subunits A, E1, and H are downregulated in ICs by ~60% in B1-deficient mice compared with B1-expressing mice. These data indicate a significant and consistent downregulation of the protein levels for these subunits. Moreover, the results of the current study correlate very well with our previously reported data showing that V-ATPase activity decreases by 60% in ICs of the outer medullary

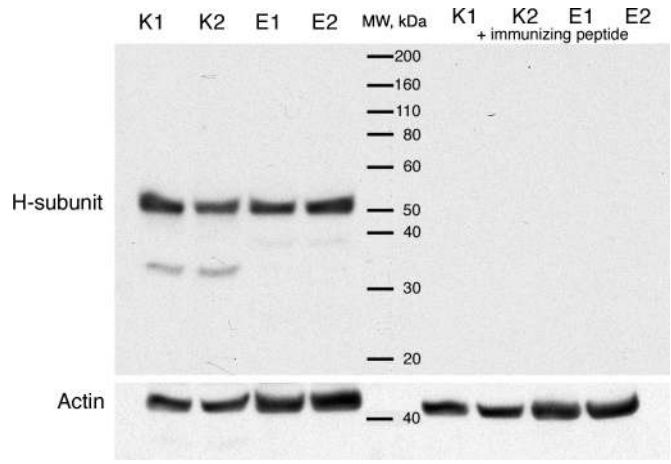

Fig. 8. Characterization of the new anti-H V-ATPase subunit (ATP6V1H) antibody. Detection of the H subunit in mouse epididymis (lanes marked E1 and E2, in which 50 μg of protein extract were loaded in each lane) and kidney (K1 and K2, 4 μg of protein extract per lane) by immunoblotting is shown. The most intense band is seen around 50 kDa, corresponding to the expected size of the H subunit (*top*). A weaker lower molecular weight band was also seen in the kidney samples. All bands were abolished when the antibody was preincubated with the immunizing peptide. Loading control was performed with an anti-actin antibody (*bottom*).

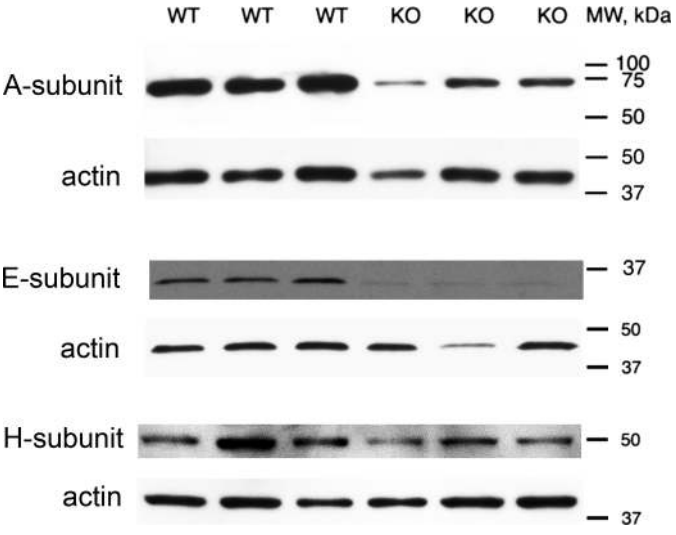

Fig. 10. Western blotting results for intercalated cell populations from 3 EGFP-B1$^{+/+}$ (WT) and 3 EGFP-B1$^{-/-}$ mice (KO). Membranes were blotted with antibodies against the V-ATPase A (ATP6V1A), E1 (ATP6V1E1), and H (ATP6V1H) subunits. The loading control performed with an anti-actin antibody is shown for each experiment. Quantification of band intensities normalized to the loading controls showed a significant reduction of all 3 subunits in B1-deficient mice compared with their B1-expressing counterparts.

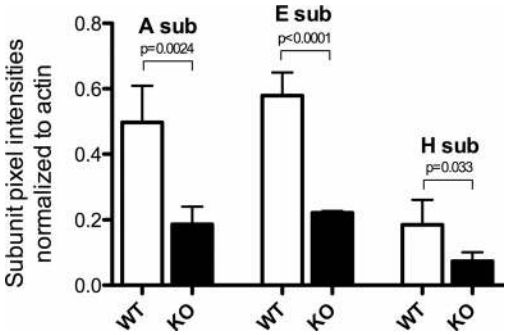

Fig. 11. Quantification of Western blotting results for intercalated cell populations from 4 EGFP-B1$^{+/+}$ (WT) and 4 EGFP-B1$^{-/-}$ mice (KO). Band intensities for the V-ATPase A (ATP6V1A), E1 (ATP6V1E1), and H (ATP6V1H) subunits are decreased by ~60% in intercalated cells from KO mice compared with WT mice, and all decreases are statistically significant, as indicated by the P values. Values are means ± SD.

(including outer and inner stripe of the OM) CDs in B1-deficient mice (38), while in the inner medullary CD ICs V-ATPase activity decreases by ~70%. Assuming that the amount of A, E1, and H subunit protein closely reflects the number of total functional V-ATPase holoenzymes, this correlation would indicate that B2-containing V-ATPases are similar to B1-containing enzymes in terms of functional efficacy, i.e., the decrease in the proton-secreting capacity of ICs in mice lacking B1 is possibly solely due to the proportional reduction in the number of V-ATPase molecules.

On the other hand, our current approach now reveals that the B2 subunit isoform is significantly upregulated in B1-deficient mice. While previously reported data, based on measurements at the whole kidney level (38), lacked the sensitivity required to detect this change, we now report that the B2-associated immunoblotting band intensity, which is indicative of B2 protein levels, is increased by ~75% in ICs from mice lacking the B1 isoform. Consequently, the increased B2 level in the IC apical membrane is not only due to a translocation of this isoform to the membrane, but ICs either produce more and/or degrade less of the B2 subunit protein. This occurs with no significant differences at the mRNA expression level in whole kidneys (38). This result suggests that a similar regulation may occur in other proton-secreting cells, such as the clear cells of the epididymis, where B1-deficient mice also show an increased membrane localization of B2-containing V-ATPases. This also occurs in the absence of a significant B2 upregulation in terms of both protein or message at the whole organ level, and in the absence of a significant change in Atp6v1b2 mRNA in microdissected epithelial cells (16). Interestingly, overexpression of an alternative isoform after knocking out another subunit is not a unique feature of ICs. Other instances have been reported when a compensating subunit is upregulated to avoid the degradation of the entire enzyme due to a lack of assembly partners. In a previous study, for example, knockout of the α1-subunit of the cerebellar GABAA receptor induced a significant reduction in the number of total receptors, whereas the amount of α6-subunit was upregulated at the protein, but not mRNA level (31).

Assuming that the measured V-ATPase subunit-associated band intensities reliably reflect their changes at the protein levels and that, in turn, changes in the ubiquitous subunits indicate similar V-ATPase quantitative changes, the numerical results describing V-ATPase downregulation and B2 subunit isoform upregulation allow an estimate of the ratio of B1- to B2-containing V-ATPases under baseline conditions. Such an estimate will be accurate if there are no "hybrid" V-ATPase assemblies in which the three B subunits in the V_1 cytosolic sector include both isoforms. Under these assumptions, the relationship equating, in Atp6v1b1$^{-/-}$ mice, 40% of the total number of functional V-ATPases in wild-type mice with 175% of B2-containing holoenzymes, yields a 3.375:1 ratio for B1- to B2-containing V-ATPases. In other words, in control animals B1 isoforms are roughly threefold more numerous than B2; i.e., ~75% of V-ATPase holoenzymes contain B1, while 25% contain B2. This information may prove useful in future studies, in which the differential regulation of B1- vs. B2-containing V-ATPases is investigated. However, should hybrid V-ATPase holoenzymes exist, in which both B1 and B2 isoforms are assembled within the same molecule, the relative contribution of the isoforms could be different.

The results in this study are consistent with the following model on V-ATPase subunit regulation in ICs from B1-deficient mice. The knockout of the B1 subunit isoform causes a significant reduction in the number of V-ATPase holoenzymes in the ICs, underlined by a substantial decrease in V-ATPase subunit protein levels for the V-ATPase subunits with no alternative isoforms in the kidney. We hypothesize that either less V-ATPase subunit protein is being produced by these cells, or it is being degraded at higher rates, possibly due to a diminished stability of the individual subunits outside of the fully assembled and functional holoenzyme. In addition, measurement of subunit mRNA levels will help to dissect the mechanisms involved.

The residual expression of the V-ATPase subunits (e.g., A, E1, and H) in B1-deficient mice is most likely reflective of

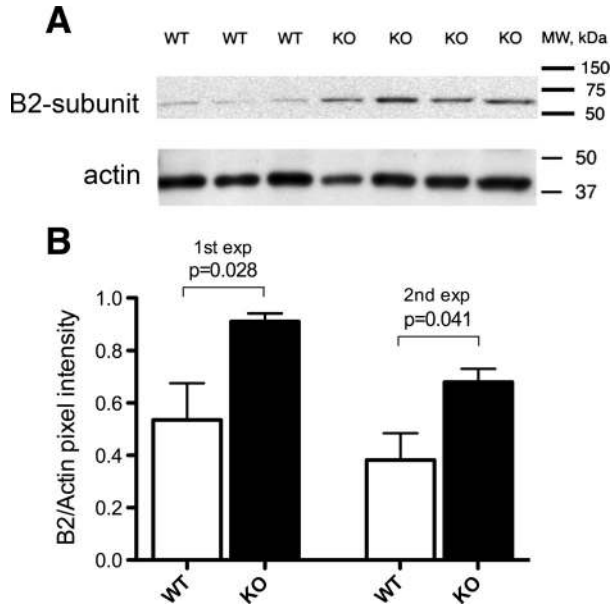

Fig. 12. Upregulation of the V-ATPase B2 subunit isoform (ATP6V1B2) in B1-deficient mice. *A*: immunoblotting results for B2 in IC from 3 EGFP-B1$^{+/+}$ (WT) and 4 EGFP-B1$^{-/-}$ mice (KO) with their respective actin loading controls. *B*: results of B2-associated band densitometry quantification from 2 different experiments, reflecting a statistically significant increase in intercalated cells from B1-deficient animals compared with their B1-expressing counterparts.

assembled V-ATPases that contain the alternative B2 subunit isoform. These B2-containing holoenzymes are similar to those present on many intracellular organelles, such as the Golgi/*trans*-Golgi network, endosomes, and lysosomes (20, 28, 30), and necessarily contain subunits with no known renal isoforms like A, E1 and H (7, 27, 41, 45). These holoenzymes could also contain various "a" isoforms, since all four isoforms were found to coimmunoprecipitate with B2 in the mouse kidney (44). This residual expression rescues the phenotype of B1-deficient mice, which appear normal as far as breeding, pup survival, growth, and gross development are concerned and present with no significant metabolic acidosis at baseline. If normal B2 levels found in wild-type animals only allow the assembly of an insufficient number of fully functional V-ATPases, ICs will consequently require increased levels of B2 protein to be maintained (by higher production rates, lower degradation rates, or both). Moreover, since most B2-containing holoenzymes are usually found associated with the membranes of intracellular organelles, the survival and quasi-normal function of B1-deficient mice necessitate holoenzyme translocation and insertion into the apical plasma membrane domain of A-ICs, thus causing the characteristic pattern of bright IC membrane staining seen in immunofluorescence assays in this study and in the preceding ones (18, 38).

The generation of new hybrid EGFP-B1$^{-/-}$ mice coupled with the sensitivity of FACS used to generate a pure population of ICs can open the doors to a series of new studies such as assessing the effect of the B1 deficiency on other transporters or relevant molecules at the protein or genomic level, unveiling some important aspects of V-ATPase endo/exocytosis, and determining the effect of drugs and hormones on various acid/base regulatory pathways. Further studies are also needed to understand the effects of the B1 deficiency in other B1-expressing tissues such as the male reproductive tract, lung, olfactory, and inner ear epithelia.

ACKNOWLEDGMENTS

The authors are grateful for the work of J. T. Rothermel, whose contribution to this study was fundamental and who sadly passed away before his time during the preparation of this paper.

GRANTS

This work was supported by National Institutes of Health (NIH) Grants DK-73266 (to T. G. Păunescu), DK-42956 (to D. Brown), DK-97124 (to S. Breton), and HD-40793 (to S. Breton) and by Swiss National Research Foundation Grant 31003A_138143/1 (to C. A. Wagner). The Microscopy Core Facility of the Program in Membrane Biology received additional support from the Boston Area Diabetes and Endocrinology Research Center (NIH DK-57521) and from the Center for the Study of Inflammatory Bowel Disease (NIH DK-43341).

DISCLOSURES

No conflicts of interest, financial or otherwise, are declared by the authors.

AUTHOR CONTRIBUTIONS

Author contributions: L.V., K.E.F., C.A.W., S.B., D.B., and T.G.P. provided conception and design of research; L.V., J.T.R., K.E.F., C.A.W., A.A., E.H., and T.G.P. performed experiments; L.V., K.E.F., C.A.W., E.H., and T.G.P. analyzed data; L.V., J.T.R., K.E.F., C.A.W., A.A., E.H., S.B., D.B., and T.G.P. interpreted results of experiments; L.V., J.T.R., K.E.F., A.A., S.B., and T.G.P. prepared figures; L.V. and T.G.P. drafted manuscript; L.V., K.E.F., C.A.W., S.B., D.B., and T.G.P. edited and revised manuscript; L.V., K.E.F., C.A.W., A.A., E.H., S.B., D.B., and T.G.P. approved final version of manuscript.

REFERENCES

1. **Alzamora R, Thali RF, Gong F, Smolak C, Li H, Baty CJ, Bertrand CA, Auchli Y, Brunisholz RA, Neumann D, Hallows KR, Pastor-Soler NM.** PKA regulates vacuolar H$^+$-ATPase localization and activity via direct phosphorylation of the a subunit in kidney cells. *J Biol Chem* 285: 24676–24685, 2010.
2. **Bastani B, Haragsim L.** Immunocytochemistry of renal H-ATPase. *Miner Electrolyte Metab* 22: 382–395, 1996.
3. **Bastani B, McEnaney S, Yang L, Gluck S.** Adaptation of inner medullary collecting duct vacuolar H-adenosine triphosphatase to chronic acid or alkali loads in the rat. *Exp Nephrol* 2: 171–175, 1994.
4. **Bastani B, Purcell H, Hemken P, Trigg D, Gluck S.** Expression and distribution of renal vacuolar proton-translocating adenosine triphosphatase in response to chronic acid and alkali loads in the rat. *J Clin Invest* 88: 126–136, 1991.
5. **Batlle D, Ghanekar H, Jain S, Mitra A.** Hereditary distal renal tubular acidosis: new understandings. *Annu Rev Med* 52: 471–484, 2001.
6. **Blair HC, Teitelbaum SL, Ghiselli R, Gluck S.** Osteoclastic bone resorption by a polarized vacuolar proton pump. *Science* 245: 855–857, 1989.
7. **Breton S, Brown D.** New insights into the regulation of V-ATPase-dependent proton secretion. *Am J Physiol Renal Physiol* 292: F1–F10, 2007.
8. **Breton S, Smith PJ, Lui B, Brown D.** Acidification of the male reproductive tract by a proton pumping H$^+$-ATPase. *Nat Med* 2: 470–472, 1996.
9. **Breton S, Wiederhold T, Marshansky V, Nsumu NN, Ramesh V, Brown D.** The B1 subunit of the H$^+$ATPase is a PDZ domain-binding protein. Colocalization with NHE-RF in renal B-intercalated cells. *J Biol Chem* 275: 18219–18224, 2000.
10. **Brown D, Bouley R, Păunescu TG, Breton S, Lu HA.** New insights into the dynamic regulation of water and acid-base balance by renal epithelial cells. *Am J Physiol Cell Physiol* 302: C1421–C1433, 2012.
11. **Brown D, Breton S.** H$^+$V-ATPase-dependent luminal acidification in the kidney collecting duct and the epididymis/vas deferens: vesicle recycling and transcytotic pathways. *J Exp Biol* 203: 137–145, 2000.
12. **Brown D, Breton S.** Mitochondria-rich, proton-secreting epithelial cells. *J Exp Biol* 199: 2345–2358, 1996.
13. **Brown D, Lydon J, McLaughlin M, Stuart-Tilley A, Tyszkowski R, Alper S.** Antigen retrieval in cryostat tissue sections and cultured cells by treatment with sodium dodecyl sulfate (SDS). *Histochem Cell Biol* 105: 261–267, 1996.
14. **Brown D, Păunescu TG, Breton S, Marshansky V.** Regulation of the V-ATPase in kidney epithelial cells: dual role in acid-base homeostasis and vesicle trafficking. *J Exp Biol* 212: 1762–1772, 2009.
15. **Da Silva N, Pisitkun T, Belleannee C, Miller LR, Nelson R, Knepper MA, Brown D, Breton S.** Proteomic analysis of V-ATPase-rich cells harvested from the kidney and epididymis by fluorescence-activated cell sorting. *Am J Physiol Cell Physiol* 298: C1326–C1342, 2010.
16. **Da Silva N, Shum WW, El-Annan J, Păunescu TG, McKee M, Smith PJ, Brown D, Breton S.** Relocalization of the V-ATPase B2 subunit to the apical membrane of epididymal clear cells of mice deficient in the B1 subunit. *Am J Physiol Cell Physiol* 293: C199–C210, 2007.
17. **Dou H, Finberg K, Cardell EL, Lifton R, Choo D.** Mice lacking the B1 subunit of H+ -ATPase have normal hearing. *Hear Res* 180: 76–84, 2003.
18. **Finberg KE, Wagner CA, Bailey MA, Păunescu TG, Breton S, Brown D, Giebisch G, Geibel JP, Lifton RP.** The B1-subunit of the H$^+$-ATPase is required for maximal urinary acidification. *Proc Natl Acad Sci USA* 102: 13616–13621, 2005.
19. **Forgac M.** Vacuolar ATPases: rotary proton pumps in physiology and pathophysiology. *Nat Rev Mol Cell Biol* 8: 917–929, 2007.
20. **Futai M, Oka T, Sun-Wada G, Moriyama Y, Kanazawa H, Wada Y.** Luminal acidification of diverse organelles by V-ATPase in animal cells. *J Exp Biol* 203: 107–116, 2000.
21. **Gong F, Alzamora R, Smolak C, Li H, Naveed S, Neumann D, Hallows KR, Pastor-Soler NM.** Vacuolar H$^+$-ATPase apical accumulation in kidney intercalated cells is regulated by PKA and AMP-activated protein kinase. *Am J Physiol Renal Physiol* 298: F1162–F1169, 2010.
22. **Hallows KR, Alzamora R, Li H, Gong F, Smolak C, Neumann D, Pastor-Soler NM.** AMP-activated protein kinase inhibits alkaline pH- and PKA-induced apical vacuolar H$^+$-ATPase accumulation in epididymal clear cells. *Am J Physiol Cell Physiol* 296: C672–C681, 2009.

23. **Herak-Kramberger CM, Breton S, Brown D, Kraus O, Sabolic I.** Distribution of the vacuolar H^+-ATPase along the rat and human male reproductive tract. *Biol Reprod* 64: 1699–1707, 2001.
24. **Hurtado-Lorenzo A, Skinner M, El Annan J, Futai M, Sun-Wada GH, Bourgoin S, Casanova J, Wildeman A, Bechoua S, Ausiello DA, Brown D, Marshansky V.** V-ATPase interacts with ARNO and Arf6 in early endosomes and regulates the protein degradative pathway. *Nat Cell Biol* 8: 124–136, 2006.
25. **Karet FE, Finberg KE, Nelson RD, Nayir A, Mocan H, Sanjad SA, Rodriguez-Soriano J, Santos F, Cremers CW, Di Pietro A, Hoffbrand BI, Winiarski J, Bakkaloglu A, Ozen S, Dusunsel R, Goodyer P, Hulton SA, Wu DK, Skvorak AB, Morton CC, Cunningham MJ, Jha V, Lifton RP.** Mutations in the gene encoding B1 subunit of H^+-ATPase cause renal tubular acidosis with sensorineural deafness. *Nat Genet* 21: 84–90, 1999.
26. **Miller RL, Zhang P, Smith M, Beaulieu V, Păunescu TG, Brown D, Breton S, Nelson RD.** V-ATPase B1-subunit promoter drives expression of EGFP in intercalated cells of kidney, clear cells of epididymis and airway cells of lung in transgenic mice. *Am J Physiol Cell Physiol* 288: C1134–C1144, 2005.
27. **Miranda KC, Karet FE, Brown D.** An extended nomenclature for mammalian V-ATPase subunit genes and splice variants. *PLoS One* 5: e9531, 2010.
28. **Nelson N, Harvey WR.** Vacuolar and plasma membrane proton-adenosinetriphosphatases. *Physiol Rev* 79: 361–385, 1999.
29. **Nelson RD, Guo XL, Masood K, Brown D, Kalkbrenner M, Gluck S.** Selectively amplified expression of an isoform of the vacuolar H^+-ATPase 56-kilodalton subunit in renal intercalated cells. *Proc Natl Acad Sci USA* 89: 3541–3545, 1992.
30. **Nishi T, Forgac M.** The vacuolar H^+-ATPases–nature's most versatile proton pumps. *Nat Rev Mol Cell Biol* 3: 94–103, 2002.
31. **Ogris W, Lehner R, Fuchs K, Furtmuller B, Hoger H, Homanics GE, Sieghart W.** Investigation of the abundance and subunit composition of GABAA receptor subtypes in the cerebellum of alpha1-subunit-deficient mice. *J Neurochem* 96: 136–147, 2006.
32. **Pastor-Soler NM, Hallows KR, Smolak C, Gong F, Brown D, Breton S.** Alkaline pH- and cAMP-induced V-ATPase membrane accumulation is mediated by protein kinase A in epididymal clear cells. *Am J Physiol Cell Physiol* 294: C488–C494, 2008.
33. **Păunescu TG, Da Silva N, Marshansky V, McKee M, Breton S, Brown D.** Expression of the 56-kDa B2 subunit isoform of the vacuolar H^+-ATPase in proton-secreting cells of the kidney and epididymis. *Am J Physiol Cell Physiol* 287: C149–C162, 2004.
34. **Păunescu TG, Da Silva N, Russo LM, McKee M, Lu HA, Breton S, Brown D.** Association of soluble adenylyl cyclase with the V-ATPase in renal epithelial cells. *Am J Physiol Renal Physiol* 294: F130–F138, 2008.
35. **Păunescu TG, Jones AC, Tyszkowski R, Brown D.** V-ATPase expression in the mouse olfactory epithelium. *Am J Physiol Cell Physiol* 295: C923–C930, 2008.
36. **Păunescu TG, Ljubojevic M, Russo LM, Winter C, McLaughlin MM, Wagner CA, Breton S, Brown D.** cAMP stimulates apical V-ATPase accumulation, microvillar elongation, and proton extrusion in kidney collecting duct A-intercalated cells. *Am J Physiol Renal Physiol* 298: F643–F654, 2010.
37. **Păunescu TG, Rodriguez S, Benz E, McKee M, Tyszkowski R, Albers MW, Brown D.** Loss of the V-ATPase B1 subunit isoform expressed in non-neuronal cells of the mouse olfactory epithelium impairs olfactory function. *PLoS One* 7: e45395, 2012.
38. **Păunescu TG, Russo LM, Da Silva N, Kovacikova J, Mohebbi N, Van Hoek AN, McKee M, Wagner CA, Breton S, Brown D.** Compensatory membrane expression of the V-ATPase B2 subunit isoform in renal medullary intercalated cells of B1-deficient mice. *Am J Physiol Renal Physiol* 293: F1915–F1926, 2007.
39. **Rothenberger F, Velic A, Stehberger PA, Kovacikova J, Wagner CA.** Angiotensin II stimulates vacuolar H^+-ATPase activity in renal acid-secretory intercalated cells from the outer medullary collecting duct. *J Am Soc Nephrol* 18: 2085–2093, 2007.
40. **Sabolic I, Brown D, Gluck SL, Alper SL.** Regulation of AE1 anion exchanger and H^+-ATPase in rat cortex by acute metabolic acidosis and alkalosis. *Kidney Int* 51: 125–137, 1997.
41. **Smith AN, Lovering RC, Futai M, Takeda J, Brown D, Karet FE.** Revised nomenclature for mammalian vacuolar-type H^+-ATPase subunit genes. *Mol Cell* 12: 801–803, 2003.
42. **Stankovic KM, Brown D, Alper SL, Adams JC.** Localization of pH regulating proteins H^+ATPase and Cl^-/HCO_3^- exchanger in the guinea pig inner ear. *Hear Res* 114: 21–34, 1997.
43. **Stover EH, Borthwick KJ, Bavalia C, Eady N, Fritz DM, Rungroj N, Giersch AB, Morton CC, Axon PR, Akil I, Al-Sabban EA, Baguley DM, Bianca S, Bakkaloglu A, Bircan Z, Chauveau D, Clermont MJ, Guala A, Hulton SA, Kroes H, Li Volti G, Mir S, Mocan H, Nayir A, Ozen S, Rodriguez Soriano J, Sanjad SA, Tasic V, Taylor CM, Topaloglu R, Smith AN, Karet FE.** Novel ATP6V1B1 and ATP6V0A4 mutations in autosomal recessive distal renal tubular acidosis with new evidence for hearing loss. *J Med Genet* 39: 796–803, 2002.
44. **Sun-Wada GH, Murata Y, Namba M, Yamamoto A, Wada Y, Futai M.** Mouse proton pump ATPase C subunit isoforms (C2-a and C2-b) specifically expressed in kidney and lung. *J Biol Chem* 278: 44843–44851, 2003.
45. **Sun-Wada GH, Tabata H, Kawamura N.** Selective assembly of V-ATPase subunit isoforms in mouse kidney. *J Bioenerg Biomembr* 37: 415–418, 2005.
46. **Toei M, Saum R, Forgac M.** Regulation and isoform function of the V-ATPases. *Biochemistry* 49: 4715–4723, 2010.
47. **Wagner CA, Finberg KE, Breton S, Marshansky V, Brown D, Geibel JP.** Renal vacuolar-ATPase. *Physiol Rev* 84: 1263–1314, 2004.
48. **Winter C, Kampik NB, Vedovelli L, Rothenberger F, Păunescu TG, Stehberger PA, Brown D, John H, Wagner CA.** Aldosterone stimulates vacuolar H^+-ATPase activity in renal acid-secretory intercalated cells mainly via a protein kinase C-dependent pathway. *Am J Physiol Cell Physiol* 301: C1251–C1261, 2011.